Progress In Electromagnetics Research M, Vol. 115, 21–34, 2023

A Gain Enhanced Dual-Band Low SAR AMC-Based MIMO Antenna for WBAN and WLAN Applications

Chengzhu Du*, Ling-Ru Pei, Jie Zhang, and Cheng-Xin Shi

Abstract—On the basis of artificial magnetic conductors (AMCs), a dual-band MIMO antenna is suggested. The proposed dual-band MIMO antenna is made up of two vertically positioned dipole antenna elements. A simple double circle-based AMC array is suggested to decrease radiation exposure to people while increasing forward gain. The antenna and the 3×3 AMC array are both printed on an FR4 substrate. The presented antenna with the AMC structure is manufactured and measured in order to confirm the simulated results in terms of S-parameters, radiation patterns, gain, and diversity parameters. The measured impedance bandwidths are 2.36–2.51 GHz and 5.03–6.12 GHz, covering WLAN and WBAN common bands (2.4–2.484 GHz, 5.15–5.875 GHz). The fabricated antenna exhibits peak gains of 3.34 dBi at 2.45 GHz and 7.48 dBi at 5.8 GHz, respectively. The SAR value of body tissue can be reduced by around 99%, while the front-to-back ratio (FBR) is noticeably enhanced. The proposed AMC-supported MIMO antenna is appropriate for WBAN and WLAN applications.

1. INTRODUCTION

In recent years, modern communication networks are developing rapidly and constantly influencing people's lives, thus more and more experts and scholars are paying attention to wireless body area networks (WBANs). As a crucial component of the fifth generation mobile communication system, WBAN is a communication network specifically designed for the human body [1]. The frequency bands for Wireless Body Area Network (WBAN) include Medical Implant Communications Services (MICSs) band (401–406 MHz), Wireless Medical Telemetry Services (WMTSs) band (420–450 MHz, 608–614 MHz, and 1.395–1.429 GHz), WLAN band (2.4–2.484 GHz and 5.15–5.875 GHz), and ultra-wideband (UWB) (3.1–10.6 GHz). When the antenna is attached to the human body, the human body will have effects on the performances of the antenna [2]. According to the radiation standards for wearable antennas set by various countries, the design antennas with low human specific absorption rate (SAR) values have attracted the attention of many researchers. Various low SAR wearable antennas have been studied with different methods [3–7]. Moreover, antennas for wearable devices must be small, light, and structurally durable [8].

Artificial magnetic conductor (AMC) is a kind of metamaterial structure, which can provide zero reflection phase for one resonant mode at one frequency [3]. Improved realized gain, lower levels of backward radiation, and an enhanced front-to-back ratio (FBR) are the results of AMC structure acting as high impedance surfaces. Recently, it can be found that AMC structures have been used to enhance the performance of antennas [3, 4, 9–14]. When an AMC reflector is attached to the antenna's rear in [3], the SAR values drop sharply from 2 to 0.29 W/kg. In [4], a 99% reduction in SAR level and low profile are obtained when the antenna is backed by an AMC array. In [11], a planar antenna integrated with a 3×3 AMC reflector can achieve a front-to-back ratio of 17.33 dB and a realized gain

Received 2 October 2022, Accepted 24 November 2022, Scheduled 7 January 2023
* Corresponding author: Chengzhu Du (duchengzhu@163.com).
The authors are with the College of Electronics and Information Engineering, Shanghai University of Electric Power, Shanghai 200090, China.

of 8 dBi. A dual-band flexible monopole antenna with an artificial magnetic conductor structure of the ISM band is proposed in [12]. The SAR is only 0.35 W/kg at 2.45 GHz and 0.39 W/kg at 5.8 GHz, and the gain is increased by more than 3.86 dBi. A wideband and high-gain microstrip-fed slot antenna based on anisotropic meta-surface (AMS) is introduced in [15], achieving a wide impedance bandwidth from 3.32 to 5.91 GHz and the peak gain of 10.7 dBi at 5.3 GHz. However, above antennas are single antenna.

Multiple-input Multiple-output (MIMO) technology has been proved a very effective way to guarantee data rates, increase system capacity, and prevent multi-path fading [16]. Recently, there have been many studies combining AMC structures with MIMO antennas, and majority of antenna systems operate in single band, dual-band, or millimeter wave wideband [17–19]. [17] introduces an integrated MIMO antenna with a 31.0% (3.0–4.1 GHz) impedance bandwidth. A dual-band MIMO antenna for 5G base station with an AMC reflector is suggested in [18]. [19] introduced a dual-band MIMO antenna integrated with AMC reflector for millimeter-wave applications. Above MIMO antennas are not suitable for WBAN application.

In this study, a two-port dual-band MIMO antenna integrated with an AMC reflector for WBAN and WLAN applications is developed. In order to increase the forward gain of the antenna and reduce the backward radiation of the antenna, a reflector has been made of a 3×3 AMC unit cell array. Both the MIMO antenna and the AMC structure are printed on an FR4 substrate. The gap between the MIMO antenna and the reflector is 10 mm. The simulation and measurement results are in good agreement. The phase analysis of the AMC structure and experimental results such as return loss, isolation, radiation patterns, peak gain, SAR, and FBR of the whole antenna system are discussed and given. To our knowledge, this may be the first study on a dual-band MIMO antenna based on an AMC structure for WBAN and WLAN communication.

2. MIMO ANTENNA CONFIGURATION

In Fig. 1, the geometrical details of MIMO antenna are depicted. The FR4 substrate, with a loss tangent of 0.02 and a relative dielectric constant of 4.4, serves as the foundation for the given dual-band MIMO antenna. The total size of the antenna is $33 \times 66 \times 0.8\,\text{mm}^3$. The manufactured antenna is displayed in Fig. 2.

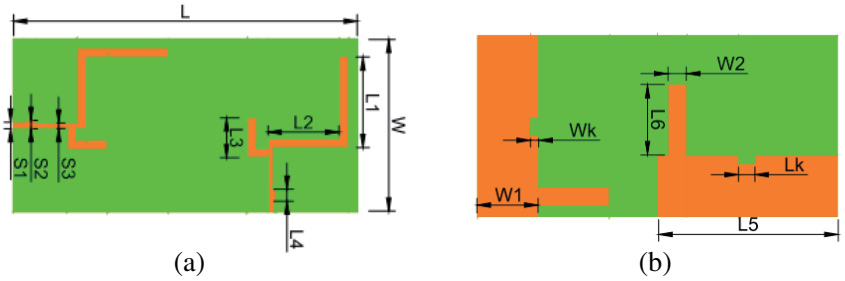

Figure 1. Geometry of the presented dual-band MIMO antenna, (a) top view, (b) back view.

To achieve good isolation, the antenna is made up of two dipole antenna elements that are positioned perpendicular to one another. Impedance matching is enhanced by using a stepped feed-line. Two protruding ground stubs are added to the ground plane to further improve the antenna's isolation. On the ground plane's edge, a tiny rectangular slot is carved for better impedance matching at high frequencies. Detailed size data of designed MIMO antenna are given below: $W = 33\,\text{mm}$, $L = 66\,\text{mm}$, $L1 = 17.58\,\text{mm}$, $L2 = 12.51\,\text{mm}$, $L3 = 7.79\,\text{mm}$, $L4 = 2.29\,\text{mm}$, $L5 = 40\,\text{mm}$, $L6 = 13\,\text{mm}$, $W1 = 11.2\,\text{mm}$, $W2 = 3.5\,\text{mm}$, $S1 = 1.26\,\text{mm}$, $S2 = 1.6\,\text{mm}$, $S3 = 1.1\,\text{mm}$, $Wk = 1.5\,\text{mm}$, $Lk = 3\,\text{mm}$.

S-parameters are measured with Agilent N5230 network analyzer. Fig. 3 displays a comparison of the simulated and measured values of the S-parameters. It can be seen from Fig. 3 that the measured results of the antenna are approximately the same as the simulation ones. The measured value of S_{11} is

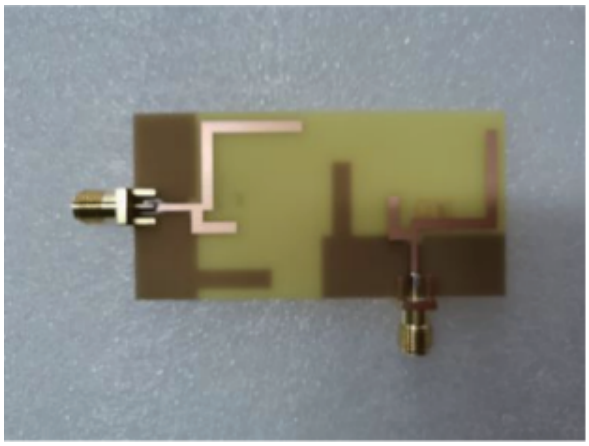

Figure 2. The manufactured MIMO antenna.

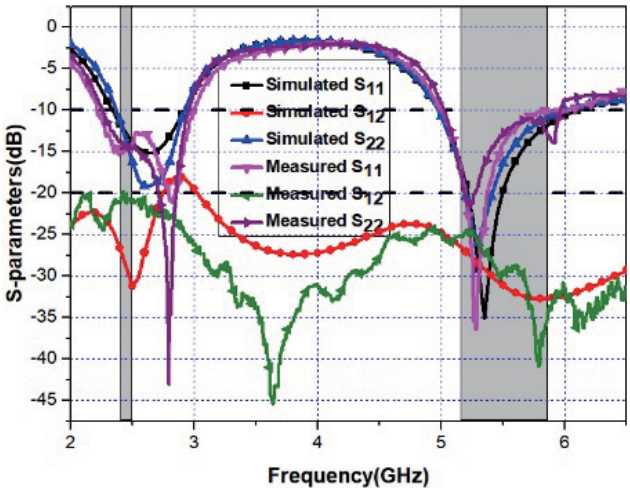

Figure 3. Simulated and measured S-parameters.

lower than -10 dB at 2.25–2.95 GHz and 5.02–5.96 GHz, which covers WLAN bands. In addition, the measured S_{12} is lower than -20 dB.

2.1. The Effects of Slot and Stub

To improve the bandwidth of the antenna, rectangular slots are etched on the ground. Fig. 4(a) shows the effect of various Wk on S_{11}. When Wk in Fig. 4(a) increases from 0 mm to 2.5 mm, the lower frequency bandwidth becomes narrower slightly, and in the higher frequency the bandwidth is wider. The optimized value of Wk is 1.5 mm, and the dual-band MIMO antenna is obtained with impedance bandwidth of 2.30–2.92 GHz and 4.95–6.18 GHz.

To improve the isolation of the antenna, rectangular stubs are added on the ground. It can be seen from Fig. 4(b) that the change of the $L6$ value has a certain impact on the isolation performance of the antenna in the dual band range. When $L6$ is 13 mm, the antenna has the best isolation performance ($S_{12} < -25$ dB) in WLAN band.

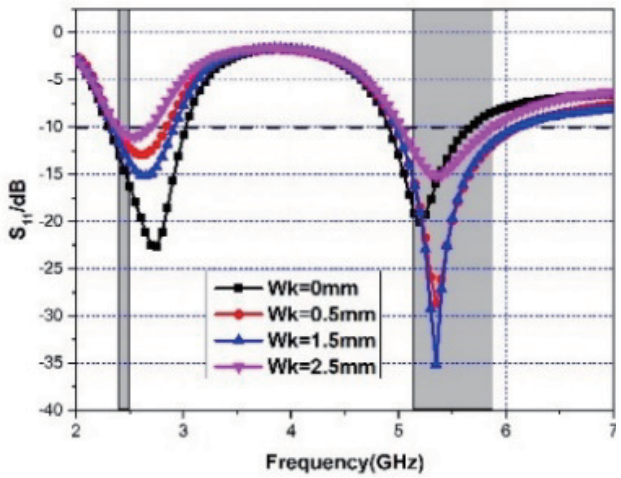

(a)

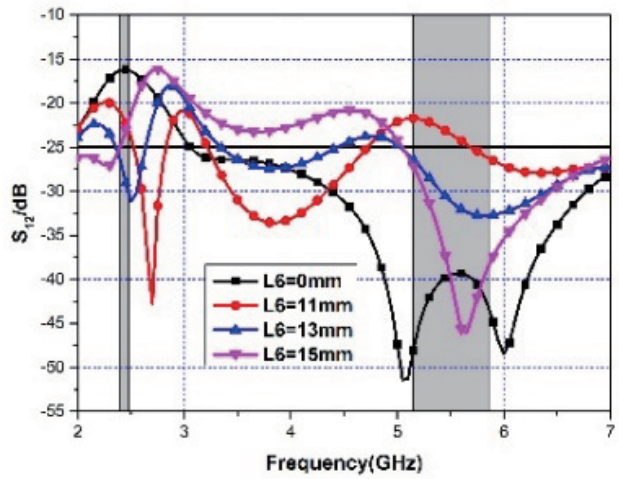

(b)

Figure 4. Simulated S-parameters effects of (a) Wk, (b) $L6$.

3. DUAL-BAND AMC DESIGN

AMC reflectors are composed of periodic unit structures. The design allows for in-phase reflection in certain frequency bands to achieve characteristics of PMC (Perfect Magnetic Conductor, PMC). PMC is a medium that does not exist in nature, and its surface impedance is infinite. By studying the impedance properties of PMC surfaces, AMC structures have been developed that can achieve PMC characteristics in certain frequency bands with in-phase reflections. The $\pm 90°$ reflected phase range is usually defined as AMC reflected phase bandwidth. The AMC generally consists of a periodic metal patch on the front of the substrate and a fully covered ground on the back of the substrate.

The AMC unit structure is illustrated in Fig. 5. The AMC unit cells are composed of a double-circular patch on the front of FR4 and metallic ground. The substrate is FR4 with a thickness H_{AMC} of 1.6 mm. The unit width is $Wamc$; $R1$ and $R2$ are the radii of the outer and inner circles, respectively; and d decides the distance between them.

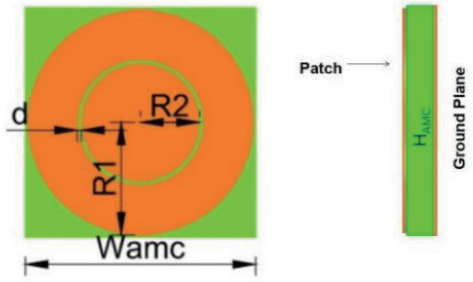

Figure 5. Structure of the AMC unit.

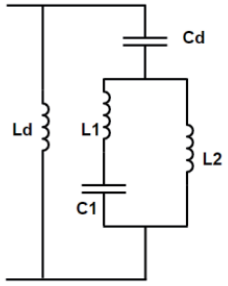

Figure 6. Equivalent circuit model of the proposed AMC structure.

The equivalent circuit model of the AMC unit is given in Fig. 6. The overall size of the AMC unit $Wamc$ determines the interval of circular periodic patch. The interval of adjacent periodic patches produces an equivalent capacitance Cd, and the short-circuited transmission line produces an equivalent inductance Ld. The circular patches with radii $R1$ and $R2$ produce equivalent inductances $L1$ and $L2$, respectively. The width on the patch of the circular slot d produces an equivalent capacitance $C1$.

The various parametric analyses of the double resonant frequencies are shown in Fig. 7. It is shown in Fig. 7(a) that lower resonance frequency will be affected when $R1$ changes. When $R1$ increases from

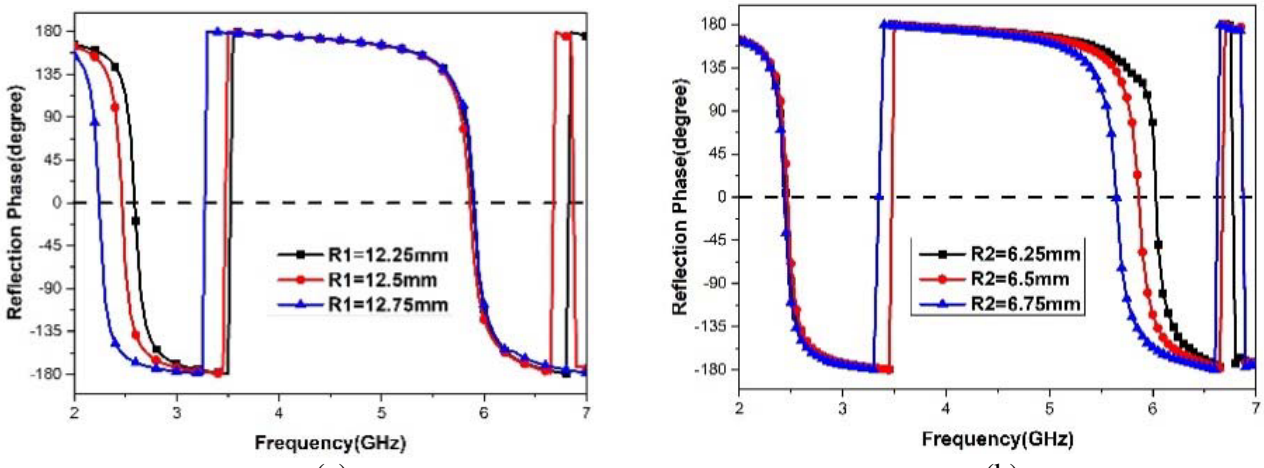

Figure 7. Reflection phases for different parameter values, (a) $R1$, (b) $R2$.

12.25 to 12.75 mm, the lower resonance frequency changes from 2.56 GHz to 2.30 GHz, but the higher resonance frequency does not shift. The optimized value of $R1$ is 12.5 mm, and the resonant frequency is 2.44 GHz. Similarly, it is shown in Fig. 7(b) that with the extension of $R2$, the higher resonance frequency changes from 6.19 GHz to 5.68 GHz, while the lower resonance frequency does not move. It can be clearly noticed that $R1$ affects the lower resonant frequency, and $R2$ is responsible for the upper resonant frequency.

The final optimized AMC dimensions are given in Table 1. The outer circular patch resonates at 2.45 GHz, and the $\pm 90^\circ$ reflection phase bandwidth is 130 MHz (2.39–2.52 GHz). The inner circular patch resonates at 5.8 GHz, and the $\pm 90^\circ$ reflection phase bandwidth is 180 MHz (5.71–5.89 GHz). Fig. 8 displays the dual-band AMC's reflection phase feature.

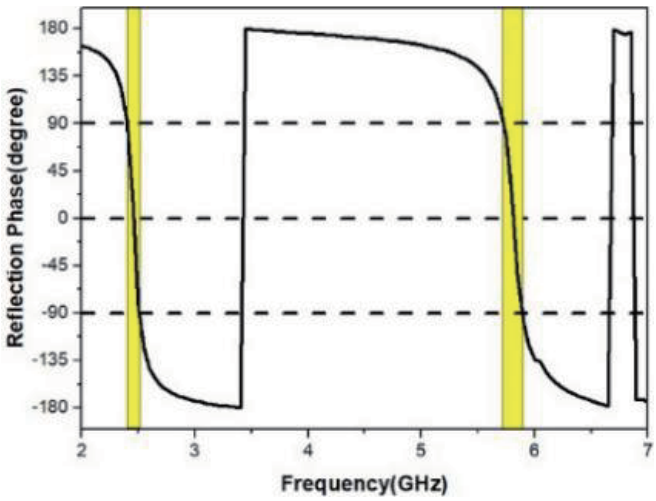

Figure 8. Reflection phase of the suggested AMC reflector.

Table 1. The parameters and dimensions of the proposed AMC unit reflector.

$Wamc$ (mm)	$R1$ (mm)	$R2$ (mm)	D (mm)
25.5	12.5	6.5	0.5

4. MIMO ANTENNA BACKED BY AMC ARRAY

Figure 9 depicts the geometry of the presented antenna over AMC arrays. To improve performance, the 3×3 AMC array is positioned as a reflector with a gap below the center of the antenna. The gap

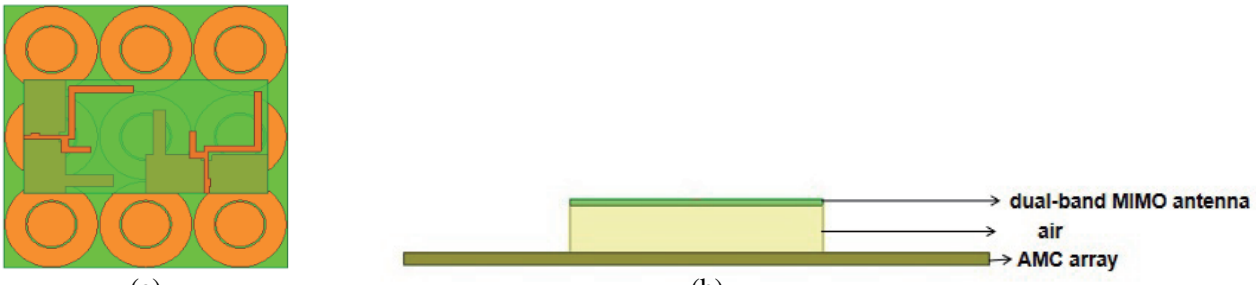

Figure 9. MIMO antenna over AMC geometric structure, (a) top view, (b) side view.

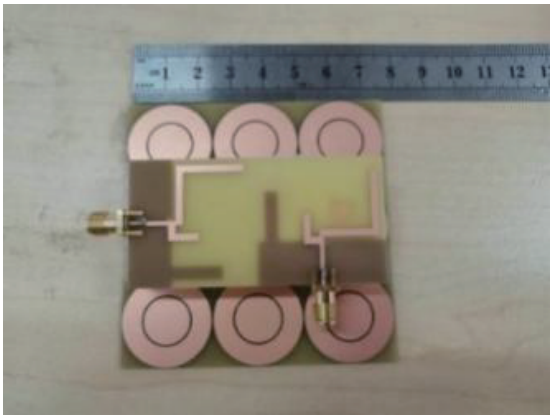

Figure 10. Fabricated AMC-backed two-element MIMO antenna.

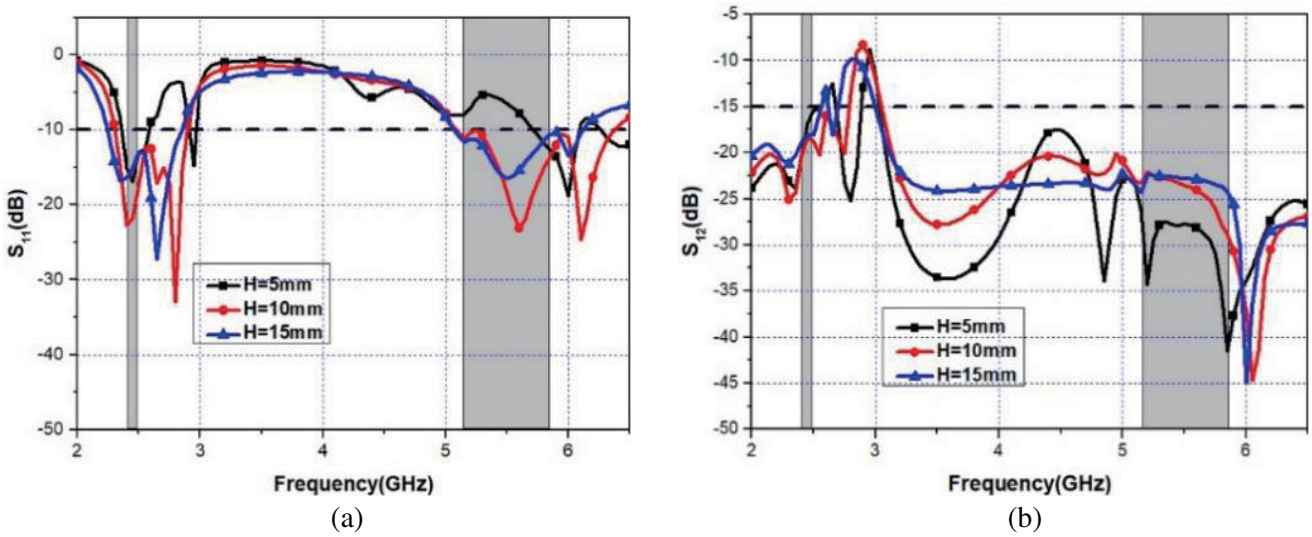

Figure 11. S-parameters for the proposed AMC-backed antenna with varying values of H, (a) S_{11}, (b) S_{12}.

parameter is H.

The design of the presented antenna supported by the 3×3 AMC structure is shown in Fig. 10. The foam is put between the AMC array and the suggested MIMO antenna, and height of the foam is 10 mm.

Figure 11 displays the S_{11} and S_{12} of the presented AMC-supported MIMO antenna with various values of H. It is clear that the value of H has strong influence on the impedance bandwidth and isolation of the MIMO antenna integrated with AMC array. In view of the AMC-supported antenna system's performance and low profile, the optimal value of H is 10 mm.

Table 2 shows simulated gains of MIMO antenna with various numbers of AMC reflectors. It is evident that the MIMO antenna has a higher gain at 5.8 GHz, when the size of AMC reflector is 3×3, and the gains are 6.96 dBi at 2.45 GHz and 6.43 dBi at 5.8 GHz.

In Fig. 12, the simulated S_{11} of the MIMO antenna supported by the AMC and PEC structure are shown for comparison study. Fig. 10 shows that when the antenna is supported by an AMC structure, the reflection coefficient is acceptable with the distance of 10 mm. The reflection coefficient is improved when the separation between antenna and PEC ground is increased from 10 mm to 40 mm. The antenna integrated with AMC reflector has a lower profile than the antenna supported by PEC reflector.

Table 2. Simulated gains of MIMO antenna with different numbers of AMC unit reflectors.

AMC array size	Frequency (GHz)	Gain (dBi)
3×2	2.45	6.4
	5.8	6.27
3×3	2.45	6.96
	5.8	6.43
4×2	2.45	6.85
	5.8	5.91
4×3	2.45	7.03
	5.8	6.15

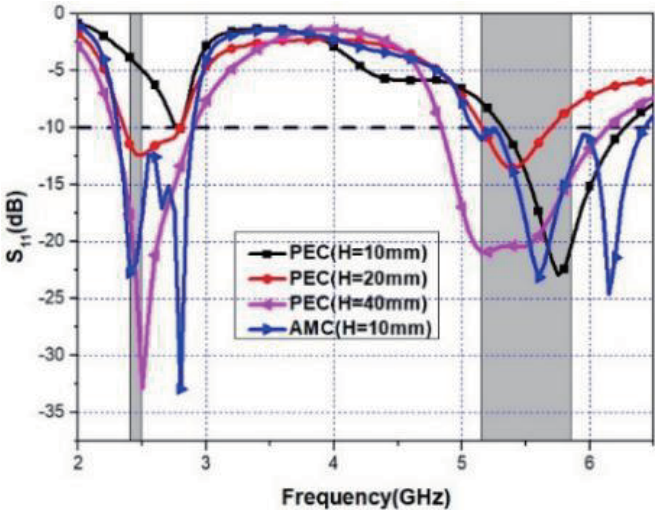

Figure 12. Simulated S_{11} of the presented antenna supported by the AMC and PEC structure.

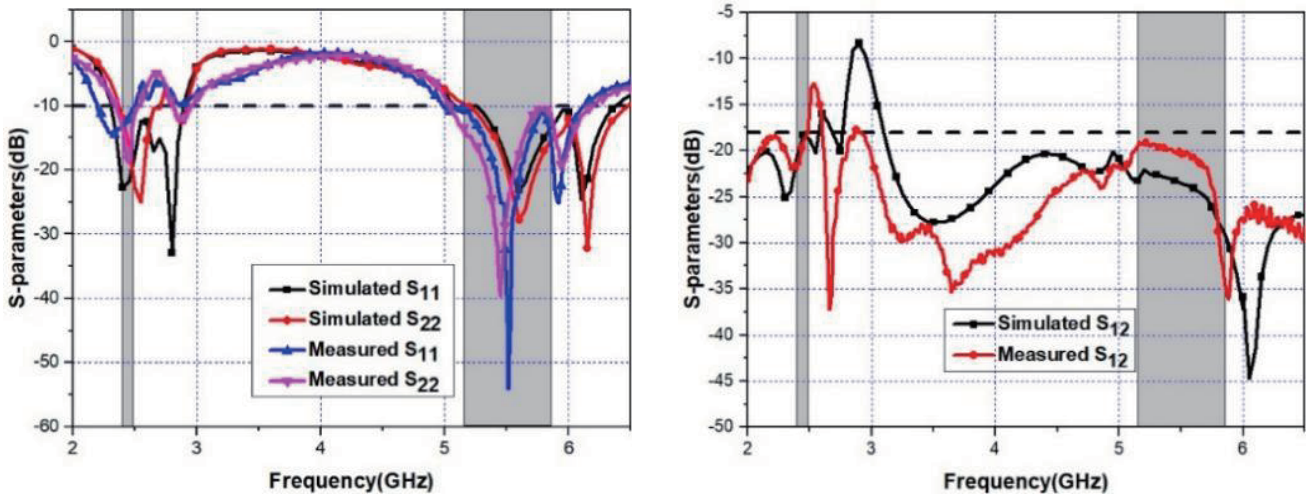

(a) (b)

Figure 13. Simulated and measured S-parameters results of the proposed AMC-supported MIMO antenna, (a) S_{11} and S_{22}, (b) S_{12}.

5. RESULTS AND EVALUATION

5.1. *S*-Parameters

Figure 13 shows the simulated and measured S_{11}, S_{12}, and S_{22} of the planned antenna. After integrating with the AMC reflector, the operating bandwidth of the whole antenna system becomes narrower. It is shown that the measured S_{11} and S_{22} operate from 2.36–2.51 GHz and 5.03–6.12 GHz. The measured isolation between elements is better than 18 dB at both bands.

5.2. Diversity Performance

Envelope correlation coefficient (ECC) and diversity gain (DG) are the key variables to gauge the extent of correlation between ports in MIMO system. The smaller the ECC is, the stronger the independence of each channel is. The ECC is calculated by *S*-parameters according to Equation (4).

$$\rho e(i,j,N) = \left| \frac{\sum_{n=1}^{N} S_{i,n}^{*} S_{n,j}}{\left| \prod_{k=i.j} \left(1 - \sum_{n=1}^{N} S_{k,n}^{*} S_{n,k} \right) \right|^{1/2}} \right|^{2} \tag{1}$$

Another more accurate way to calculate the ECC value is by applying the far field radiation of the antennas using the following Equation (5). Moreover, the ECC is required to be less than 0.5 to ensure the antenna performance.

$$\rho e = \frac{\left| \int\int \left[\vec{F}1(\theta,\varphi) \times \vec{F}2(\theta,\varphi) \right] d\Omega^{2} \right|}{\int\int \left| \vec{F}1(\theta,\varphi) \right|^{2} d\Omega \int\int \left| \vec{F}2(\theta,\varphi) \right|^{2} d\Omega} \tag{2}$$

Diversity gain is a index to evaluate the correlation of MIMO antenna radiation patterns, and it can be calculated by Equation (6).

$$\mathrm{DG} = 10\sqrt{1 - ECC^{2}} \tag{3}$$

Figure 14 shows ECC and DG results of the proposed AMC-backed antenna. Measured ECC from *S*-parameter is lower than 0.01, and the DG level of antenna is excellent, which is better than 9.99

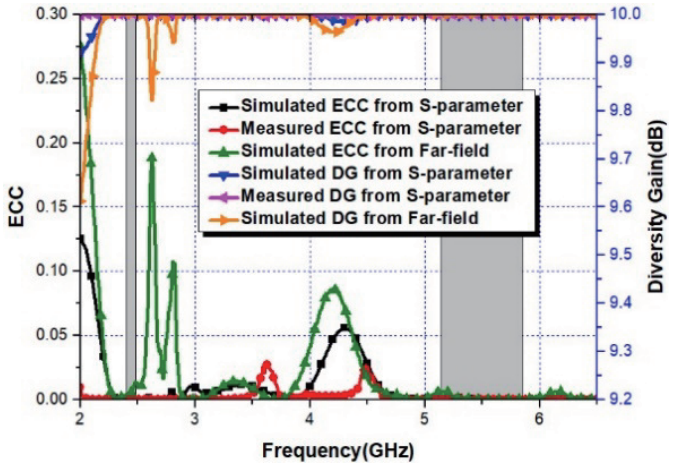

Figure 14. Simulated and measured ECC and DG results of the suggested antenna system.

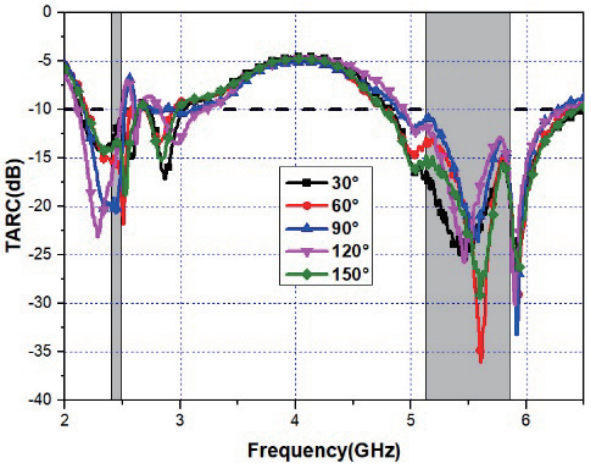

Figure 15. Measured curves of TARC in different degrees.

within WLAN bands. As a result, the analysis of ECC and DG values supports the excellent diversity capability of the provided MIMO antenna system.

Another fundamental parameter that forecasts the behavior of the entire MIMO system is total active reflection coefficient (TARC). The TARC can be calculated as:

$$\text{TARC} = N^{-0.5}\sqrt{\sum_{i=1}^{N}\left|\sum_{k=1}^{N}|Sike^{j\theta k-1}|\right|^2} \tag{4}$$

θ represents the angle of the excitation phase. The angles chosen in this article to analyze the provided MIMO antenna's characteristics are 30°, 60°, 90°, 120°, and 150°. Fig. 15 displays the measured TARC curves for the range of 2–6.5 GHz. It is obvious that the measured TARC value is below −10 dB over the 2.19–2.50 GHz and 4.94–6.27 GHz frequency bands, covering WLAN bands.

Channel capacity loss (CCL) is used to describe the message transmission rate in communication systems, and the CCL of MIMO antennas should be less than 0.4 bits/s/Hz within the operating bandwidth. The CLL can be calculated as:

$$\text{CCL} = -\log 2\det(a^R) \tag{5}$$

$$a^R = \begin{bmatrix} a11 & a12 & a13 & a14 \\ a21 & a22 & a23 & a24 \\ a31 & a32 & a33 & a34 \\ a41 & a42 & a43 & a44 \end{bmatrix}, \quad aii{=}1 - \left(\sum_{j=1}^{N}|Sij|^2\right) \quad \text{and} \quad aij = -(S^*iiSij + S^*jiSij) \tag{6}$$

Within the operational frequency band, the proposed two-port MIMO antenna system's CCL is less than 0.4 bits/s/Hz, as illustrated in Fig. 16. These four parameters guarantee the good MIMO performance of the proposed dual-band MIMO antenna backed by an AMC structure.

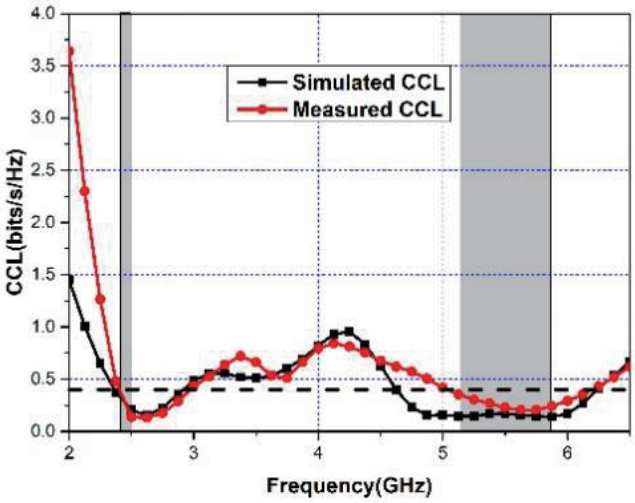

Figure 16. Simulated and measured CLL results of the suggested antenna system.

5.3. Radiation Pattern, Gain and FBR

The co-polar normalized radiation patterns of proposed antenna with and without an AMC structure are simulated and measured at E-plane and H-plane.

In Fig. 17, when the AMC reflector is loaded under the MIMO antenna, the front-to-back ratio of the radiation patterns increases significantly.

The simulated and measured gains of antenna with and without an AMC structure are depicted in Fig. 18. Comparing simulation results with measurement ones, the gain of antenna with an AMC

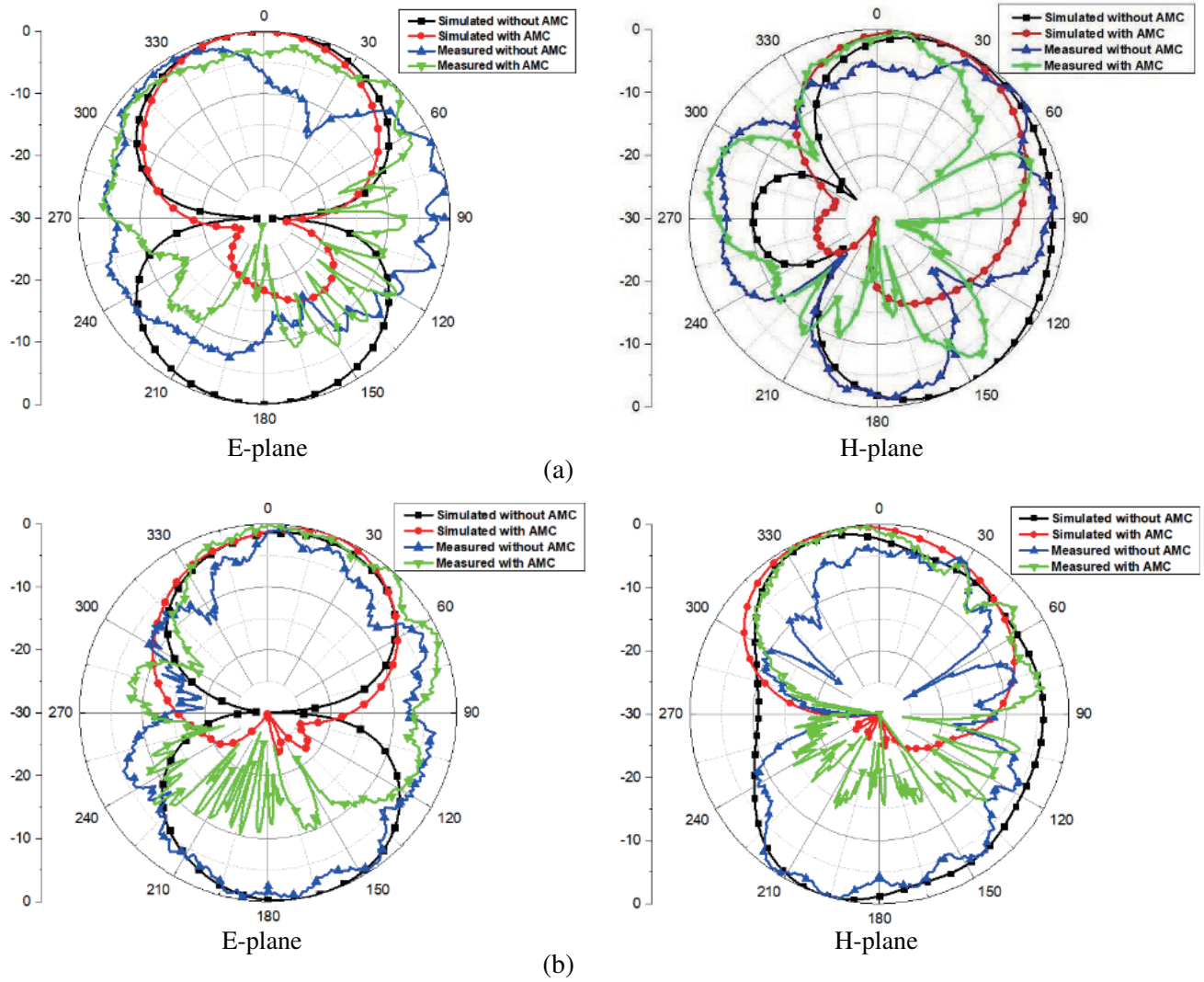

Figure 17. Simulated radiation patterns of the two-element MIMO antenna with and without AMC reflector, (a) 2.45 GHz, (b) 5.8 GHz.

structure is higher than that without an AMC structure. With AMC reflector, the measured antenna gain is 3.34 dB and 7.48 dB at lower and higher operating frequencies.

For wearable antennas, a larger FBR will achieve a lower radiation back to human body, which means that the antenna has higher safety. Table 3 shows an FBR comparison of two-element MIMO antenna with and without an AMC structure. It is obvious that the FBR values of the antenna with an AMC structure are 18.6 dB at 2.45 GHz and 26.77 dB at 5.8 GHz.

Table 3. A comparison of FBR between antenna with and without AMC structure.

Frequency (GHz)	FBR of antenna without AMC structure (dB)	FBR of antenna with AMC structure (dB)
2.45	1.048	18.60
5.8	4.55	26.77

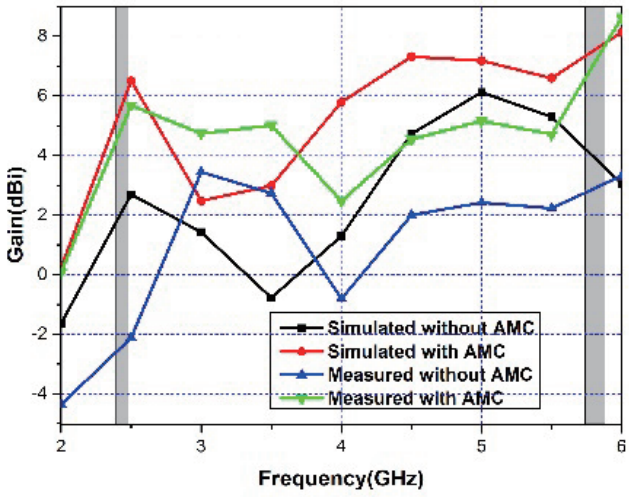

Figure 18. Simulated and measured gains of the MIMO antenna with and without AMC structure.

5.4. On Body Effects of the MIMO Antenna System

To study on-body effects on the MIMO antenna, the S-parameters are measured when the MIMO antenna supported by AMC reflector is attached to the different body tissues, as shown in Fig. 19. Although compared with the results of the antenna off-body, measured results of the antenna on human tissues have slight deviations, in the WLAN band (2.4–2.484 GHz, 5.15–5.875 GHz), S_{11} is less than -8 dB, and S_{12} is less than -15 dB, which meets the actual engineering requirements.

Specific absorption ratio (SAR) is typically used by flexible antennas to evaluate the radiation energy on human body tissue. For the U.S. standard and EU standard, the SAR level should be kept below 1.6 W/kg per 1 g of tissue and below 2 W/kg per 10 g of tissue, respectively [20]. The formula for determining SAR is as follows:

$$SAR = \frac{\sigma E^2}{\rho} \tag{7}$$

where ρ represents the mass density, E the electric field intensity, and σ the conductivity of human

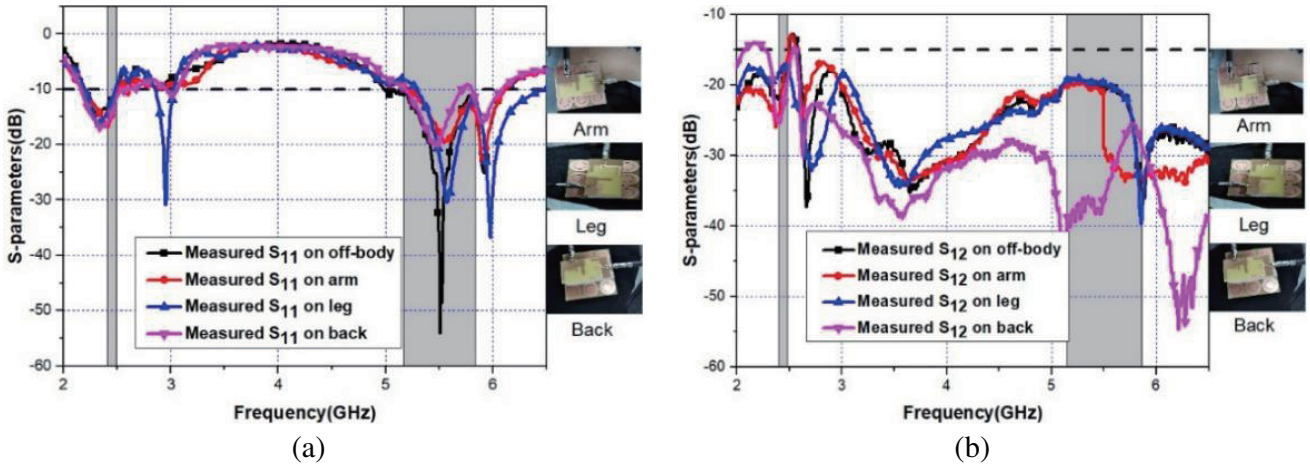

Figure 19. The S-parameters of the suggested AMC-integrated antenna on human body, (a) S_{11}, (b) S_{12}.

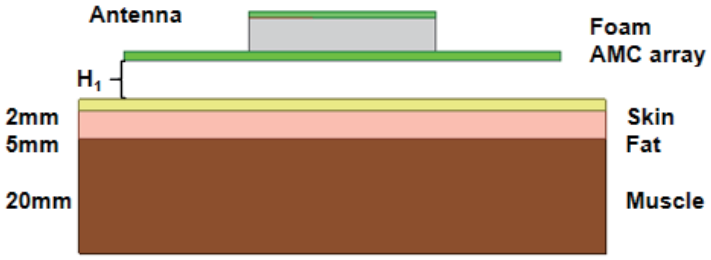

Figure 20. The human body tissue approaching the antenna model.

tissue.

The human tissue model used in this study, which has layers of skin, fat, and muscle, is depicted in Fig. 20. In Table 4, the specifications for each layer of body tissue are displayed.

Setting the input power as 0.1 W and setting 2.45 GHz and 5.8 GHz as the center frequency, respectively, the SAR values of antenna with and without an AMC reflector are simulated by HFSS. The maximum SAR values of 10 g body tissue are displayed in Table 5. According to the simulated data, the maximum simulated SAR values of AMC-integrated antennas are significantly lower than those of antennas without AMC structures, and they all meet the EU standard of 2 W/kg/10 g tissue.

Table 4. The parameters of human tissue.

	Skin	Fat	Muscle
ε_r	37.95	5.27	52.67
σ (S/m)	1.45	0.11	1.77
Density (kg/m^3)	1001	900	1006
Thickness (mm)	2	5	20

Table 5. Comparison of maximum SAR of MIMO antenna with and without AMC array.

MIMO antenna	$H1$ (mm)	Frequency (GHz)	Max SAR (W/Kg)
Without AMC structure	0	2.45	4.2864
		5.8	4.9475
	3	2.45	1.8553
		5.8	2.5113
	6	2.45	1.9688
		5.8	1.4419
With AMC structure	0	2.45	0.1175
		5.8	0.1697
	3	2.45	0.0068
		5.8	0.0018
	6	2.45	0.0059
		5.8	0.0020

6. PERFORMANCE COMPARISON

Table 6 shows a performance comparison with earlier publications. It is clear that the introduced dual-band AMC-backed MIMO antenna performs well, offering high isolation, high gain, high FBR, and low SAR. As a result, the antenna system can be widely used in WBAN and WLAN applications.

Table 6. Comparison of the designed antenna with other reported antennas.

Ref	Num of elements	Substrate	f (GHz)	Gain (dBi)	Isolation (dB)	Size (mm^2)	Max.SAR (W/kg)
[3]	1	Rogers RO3003	2.45/3.3	6.4		88.75×82.5	0.29
[4]	1	Rogers RO3003	3.5/3.8	9.373	-	86×86	0.333
[5]	1	PDMS and AgNWs	2.4	5.2		50×50	0.18
[6]	1	Rogers RO3003	2.38	6.2	-	62×42	0.66
[12]	1	Polyimide	2.45/5.8	6.89	-	61.5×61.5	0.39
[18]	2	FR4	3.5/4.7	8.2	< -20	79.6×79.6	
This work	2	FR4	2.45/5.8	7.48	< -18	76.5×76.5	0.16

7. CONCLUSION

A two-port dual-band AMC-supported MIMO antenna system is proposed. The antenna works at 2.36–2.51 GHz and 5.03–6.12 GHz, which covers WBAN and WLAN bands. By introducing an annular AMC array underneath the MIMO antenna, the gain enhancement of 5.48 dBi and 4.31 dBi is observed at 2.45 GHz and 5.8 GHz, respectively. A very low SAR is achieved, and the antenna system can operate with a high front-to-back ratio within 2.45 GHz and 5.8 GHz bands. The simulation and measurement results of the MIMO antenna systems confirm that high isolation and low correlation are obtained. The dual-band MIMO antenna supported by AMC reflector is appropriate for WBAN and WLAN applications.

REFERENCES

1. Astrin, A. W., H.-B. Li, and R. Kohno, "Standardization for body area networks," *IEIC Transactioon Communications*, Vol. 92-B, 366–372, 2009.
2. Mäkinen, R. M. and T. Kellomäki, "Body effects on thin single-layer slot, self-complementary, and wire antennas," *IEEE Transactions on Antennas and Propagation*, Vol. 62, No. 1, 385–392, 2014.
3. Saeed, S. M., C. A. Balanis, C. R. Birtcher, A. C. Durgun, and H. N. Shaman, "Wearable flexible reconfigurable antenna integrated with artificial magnetic conductor," *IEEE Antennas and Wireless Propagation Letters*, Vol. 16, 2396–2399, 2017.
4. El Atrash, M., M. A. Abdalla, and H. M. Elhennawy, "A wearable dual-band low profile high gain low SAR antenna AMC-backed for WBAN applications," *IEEE Transactions on Antennas and Propagation*, Vol. 67, No. 10, 6378–6388, 2019.
5. Jiang, Z. H., Z. Cui, T. Yue, Y. Zhu, and D. H. Werner, "Compact, highly efficient, and fully flexible circularly polarized antenna enabled by silver nanowires for wireless body-area networks," *IEEE Transactions on Biomedical Circuits and Systems*, Vol. 11, No. 4, 920–932, 2017.
6. Jiang, Z. H., D. E. Brocker, P. E. Sieber, and D. H. Werner, "A compact, low-profile metasurface-enabled antenna for wearable medical body area network devices," *IEEE Transactions on Antennas and Propagation*, Vol. 62, No. 8, 4021–4030, 2014.
7. Kitra, M. I., P. McEvoy, J. C. Vardaxoglou and J. R. James, "Material loaded antennas and their contribution towards low-SAR," *2004 IEE Antenna Measurements and SAR, AMS 2004*, 75–78, 2004.

8. Liu, H., J. Wang, and X. Luo, "Flexible and compact AMC based antenna for WBAN applications," *2017 IEEE International Symposium on Antennas and Propagation & USNC/URSI National Radio Science Meeting*, 587–588, 2017.
9. Pandit, V. K. and A. R. Harish, "Gain enhancement of a dual-band monopole antenna loaded with dual-band AMC," *2017 IEEE Applied Electromagnetics Conference (AEMC)*, 1–2, 2017.
10. Mumin, A. R. O., R. Alias, J. Abdullah, S. H. Dahlan, J. Ali, and S. K. Debnath, "Design a compact square ring patch antenna with AMC for SAR reduction in WBAN applications," *Bulletin of Electrical Engineering and Informatics*, Vol. 9, No. 1, 370–378, 2020.
11. Bahaa Qas Elias, B., P. Jack Soh, A. Abdullah Al-Hadi, C. Hodgkinson, and S. K. Podilchak, "Design of a compact textile crown antenna integrated with AMC for wearable iot applications," *2021 15th European Conference on Antennas and Propagation (EuCAP)*, 1–4, 2021.
12. Wang, S. and H. Gao, "A dual-band wearable conformal antenna based on artificial magnetic conductor," *International Journal of Antennas and Propagation*, Vol. 2022, Article ID 9970477, 8 pages, 2022.
13. Gong, Y., S. Yang, B. Li, Y. Chen, F. Tong, and C. Yu, "Multi-band and high gain antenna using AMC ground characterized with four zero-phases of reflection coefficient," *IEEE Access*, Vol. 8, 171457–171468, 2020.
14. Chaouche, Y. B. and M. Nedil, "A compact CP wearable antenna backed by AMC array for WBAN/WLAN applications," *2022 IEEE International Symposium on Antennas and Propagation and USNC-URSI Radio Science Meeting (AP-S/URSI)*, 1882–1883, 2022.
15. Zhou, E., Y. Cheng, F. Chen, H. Luo, and X. Li, "Low-profile high-gain wideband multi-resonance microstrip-fed slot antenna with anisotropic metasurface," *Progress In Electromagnetics Research*, Vol. 175, 91–104, 2022.
16. Yang, Z., F. Li, X. Yang, and F. Li, "A compact dual-band MIMO antenna with high isolation for WLAN applications," *2018 48th European Microwave Conference (EuMC)*, 1125–1128, 2018.
17. Zhu, J., S. Li, S. Liao, and Q. Xue, "Wideband low-profile highly isolated MIMO antenna with artificial magnetic conductor," *IEEE Antennas and Wireless Propagation Letters*, Vol. 17, No. 3, 458–462, 2018.
18. Liu, Q., H. Liu, W. He, and S. He, "A low-profile dual-band dual-polarized antenna with an AMC reflector for 5G communications," *IEEE Access*, Vol. 8, 24072–24080, 2020.
19. Ibrahim, A. A. and W. A. E. Ali, "High gain, wideband and low mutual coupling AMC-based millimeter wave MIMO antenna for 5G NR networks," *AEU — International Journal of Electronics and Communications*, Vol. 142, 2021.
20. Du, C., X. Li, and S. Zhong, "Compact liquid crystal polymer based tri-band flexible antenna for WLAN/ WiMAX/5G applications," *IEEE Access*, 2019.